Attitude Control for a Pectoral Fin Actuated Bio-inspired Robotic Fish

Giovanni Barbera, Lijuan Pi and Xinyan Deng

***Abstract*— In this work we present a dynamic model for a pectoral fin driven robotic fish, simple yet precise enough to be successfully implemented on a Bio-inspired Underwater Vehicle with multiple fins, modeled after the *Ostracion Meleagris*, a coral reef dweller well known for its surprising maneuverability and dynamic stability. The control algorithm relies on a robust and computationally efficient sensory feedback, based on a complementary filter fusing data from different Inertial Measurement Unit (IMU) sensors. The almost global stability of the attitude estimator guarantees convergency and robustness to noise and parameters uncertainties, showing good performance of the vehicle in steering plane maneuvering. First, the controller was implemented to do point-to-point tracking of a desired roll angle while the robot was tethered. It was then implemented in a freely swimming robot to do trajectory tracking of a desired sinusoidal roll angle. Finally, to demonstrate the effectiveness of the combined roll/yaw coupling on the maneuverability of the robot, the freely swimming robot was controlled to perform banked turns to circle the tank in loops.**

I. INTRODUCTION

Over the last two decades marine locomotion has been an active area of research for both engineers and biologists [1], [2], [3]. The interest in Autonomous Underwater Vehicles (AUVs) is to be attributed to the large number of practical purposes, which range from ocean exploration, to surveillance, wrecks inspection or offshore platforms maintenance.

A small, maneuverable autonomous underwater vehicle would be particularly useful for operations in cluttered or dangerous environments; moreover, its silent propulsion mechanism makes the robot much more difficult to detect than usual rotary propelled vehicles, allowing at the same time a good integration with underwater habitat for the collection of biological data with the lowest environmental impact.

Aquatic animal locomotion systems, based on a five hundred million year evolution and continuous improvement by natural selection, has been a constant source of inspiration for engineers. New trends in robotics are heading toward the design of bio-inspired models, especially for aerial and aquatic locomotion: based on the observation of fish, insects, and birds behavior, new kinds of propellers and actuators have been proposed: Tangorra *et al.* [4] developed an accurate model of pectoral fin capable of mimicking the kinematics of the bluegill sunfish pectoral fin during turning maneuvers; in [5] Low *et al.* implemented a spherical joint to drive a pair of pectoral fins with a combined rowing-flapping-feathering motion. More recently, the introduction of smart materials such as ionic polymer-metal composites (IPMC) [6] and shape memory alloys (SMA) wires [7], [8], [9] greatly expanded the actuator design possibilities, by making possible the reproduction of highly complex and varied kinematic patterns, and thus enabling to exploit more sophisticated ways controlling the flow around the vehicle for propulsion, maneuvering and control. In the present work, we present our recent results on the sensory feedback attitude control of a bio-inspired robotic fish with pectoral fin actuation.

G. Barbera and X. Deng are with the Department of Mechanical Engineering of Purdue University, West Lafayette, IN 47907, USA. gbarbera@purdue.edu, xdeng@purdue.edu

L. Pi is with the Department of Mechanical Engineering of University of Delaware, Newark, DE 19716, USA.

II. PECTORAL FIN LOCOMOTION

Pectoral fins play an important role both for thrust production − especially among Median and Paired Fin (MPF) swimmers [2], [10], [11] − and for steering and maneuvering (in some species for braking and reverse swimming as well). In fact, even just for hovering, every fish must oscillate its pectoral fins to correct its intrinsic instability [3].

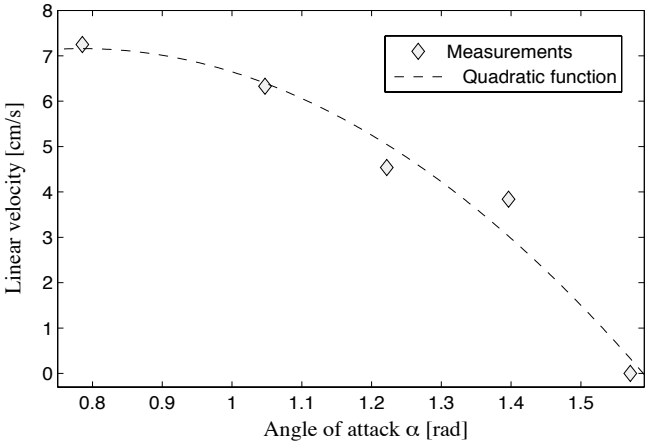

Fig. 1: AUV linear velocity vs pectoral fins angle of attack. The measures were taken along a 75cm long path, with fins beating at 3Hz.

One of the main shortcomings of caudal fin propulsion is the recoil movement which inevitably affects the attitude of the vehicle, especially in the yaw plane. Differently, a pectoral fin based propulsion would not suffer this kind of problem, since the symmetric force generation compensates for and balances the yaw plane recoil movements. In particular, the thrust produced depends on the angle of attack of the fins. We started by experiments with angles of attack varying between 0 and $\pi/2$, while the pectoral

fins beat at 3Hz with amplitude $A = \pi/4$, and the results are shown in Fig. 1. By increasing the angle of attack the thrust efficiency is reduced, whereas maneuverability and roll controllability increase significantly. This fact is confirmed by the experimental results shown in Fig. 2: the roll angle convergency to the reference is faster as the angle of attack increases.

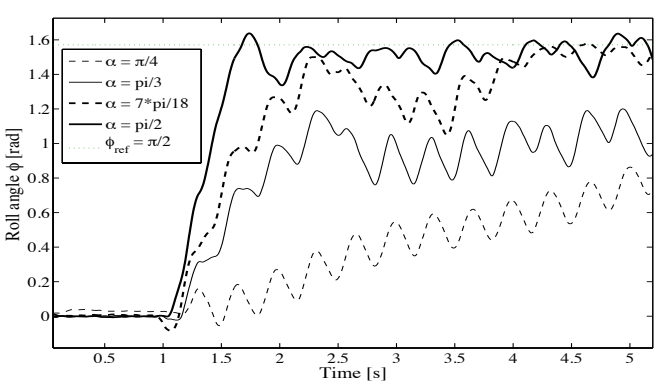

Fig. 2: Rolling angles ϕ in four different experiments, where the angles of attack α were varied in the range $\pi/4 \div \pi/2$, and the reference roll angle was set to $\phi_{ref} = \pi/2$. Between $t_0 = 0$s and $t_1 = 1$s an automatic calibration was performed on the AUV sensors.

III. Dynamic model

The robot is modeled as a rigid body with three appendages (pectoral and caudal fins) surrounded by an irrotational, inviscid, incompressible fluid. Its motion is the 3-D space is described through its 3 rotational and 3 translational degrees of freedom, with a set of nonlinear, first-order differential equations. For convenience the dynamics equations are considered with respect to the body-fixed frame, thus, combining Newton's second law for linear motion and Euler's equation for angular motion, one gets:

$$\begin{bmatrix} mI & 0 \\ 0 & \mathcal{I} \end{bmatrix} \begin{bmatrix} \dot{\mathbf{v}}^b \\ \dot{\boldsymbol{\omega}}^b \end{bmatrix} + \begin{bmatrix} \boldsymbol{\omega}^b \times m\mathbf{v}^b \\ \boldsymbol{\omega}^b \times \mathcal{I}\boldsymbol{\omega}^b \end{bmatrix} = \begin{bmatrix} \mathbf{f}^b \\ \boldsymbol{\tau}^b \end{bmatrix} \quad (1)$$

being m the mass of the robot, $I \in \mathbb{R}^{3\times3}$ the identity matrix, $\mathbf{v}^b$ and $\boldsymbol{\omega}^b$ respectively the linear and angular velocity in the body-fixed frame, $\mathcal{I}$ the inertia tensor (relative to the body frame), and $\mathbf{f}^b$ and $\boldsymbol{\tau}^b$ the external force and torque, applied to the center of mass of the robot; the cross products represent the Coriolis effect due to the fact that $\{\mathcal{B}\}$ is not an inertial frame.

By exploiting the symmetric properties of the inertia tensor $\mathcal{I}$ it is possible to expand Eq. 1 as:

$$\begin{cases} m(\dot{u} - rv + qw) &= f_x \\ m(\dot{v} + ru - pw) &= f_y \\ m(\dot{w} - uq + pv) &= f_z \\ I_{xx}\dot{p} + rq(I_{zz} - I_{yy}) + I_{xz}(\dot{r} + qp) &= \tau_x \\ I_{yy}\dot{q} + rp(I_{xx} - I_{zz}) + I_{xz}(r^2 - p^2) &= \tau_y \\ I_{zz}\dot{r} + qp(I_{yy} - I_{xx}) + I_{xz}(\dot{p} - qr) &= \tau_z \end{cases} \quad (2)$$

where the external forces in the right hand side of the above set of equations comprise hydrostatic forces (i.e. gravity and buoyancy) hydrodynamic (including body drag and added mass effects) and control forces (determined by the hydrodynamics of flapping fins).

By expanding those terms it is possible to write the extended Newton-Euler dynamic equation:

$$\begin{aligned} \mathcal{M}\begin{bmatrix} \dot{\mathbf{v}}^b \\ \dot{\boldsymbol{\omega}}^b \end{bmatrix} + \Big(\mathcal{C}_a - \mathcal{D}_L\Big)\begin{bmatrix} \mathbf{v}^b \\ \boldsymbol{\omega}^b \end{bmatrix} + \begin{bmatrix} \boldsymbol{\omega}^b \times m\mathbf{v}^b \\ \boldsymbol{\omega}^b \times \mathcal{I}\boldsymbol{\omega}^b \end{bmatrix} + \\ -\mathcal{D}_Q\begin{bmatrix} |\mathbf{v}^b|\,\mathbf{v}^b \\ |\boldsymbol{\omega}^b|\,\boldsymbol{\omega}^b \end{bmatrix} = \begin{bmatrix} (m - \rho V)R^T\mathbf{g} \\ \mathbf{x}_b \times \rho V R^T\mathbf{g} \end{bmatrix} + \\ + \begin{bmatrix} I & 0 \\ \hat{\mathbf{r}}_{CM} & I \end{bmatrix}\begin{bmatrix} \mathbf{f}_p^f(\alpha,\beta,\dot{\beta}) \\ \boldsymbol{\tau}_p^f(\alpha,\beta,\dot{\beta}) \end{bmatrix} \end{aligned} \quad (3)$$

being $\mathcal{M} = \mathcal{M}_b + \mathcal{M}_a$ the mass and inertia matrix (including added mass), and $\mathcal{D}_L$ and $\mathcal{D}_Q$ respectively the linear and quadratic drag coefficient matrices.

As a first step, a simple decoupled model for the roll dynamics is derived from Eq. 3 and successively validated through experimental data (see Section IV). By setting the pitch and yaw rate $\dot{\theta} = \dot{\phi} = 0$ and the pitch angle $\theta = 0$ one gets the following dynamics:

$$(I_{xx} + m_{44})\dot{p} = k_p p + k_{|p|p}|p|p - \rho V g z_b \sin\phi + \tau_x \quad (4)$$

where τ_x indicates the control torque applied through pectoral fins. For small perturbations about $\phi = 0$ (which is a typical operating point for many AUVs) it is possible to consider the linearized system:

$$\begin{bmatrix} \dot{p} \\ \dot{\phi} \end{bmatrix} = \begin{bmatrix} \frac{k_p}{I_{xx}+m_{44}} & \frac{-\rho V g z_b}{I_{xx}+m_{44}} \\ 1 & 0 \end{bmatrix}\begin{bmatrix} p \\ \phi \end{bmatrix} + \begin{bmatrix} \frac{1}{I_{xx}+m_{44}} \\ 0 \end{bmatrix}\tau_x \quad (5)$$

Since the linear drag coefficient k_p is negative, by applying Routh stability criterion it is clear that the stability of the system described by Eq. 5 only depends on the relative position of the center of buoyancy with respect to the center of mass: for $z_b > 0$ the equilibrium point $\phi = 0$ is asymptotically stable whereas $\phi = \pi/2$ is unstable; conversely, for $z_b > 0$ (i.e. if the center of buoyancy lies below the center of gravity), the equilibrium property is inverted. Thus, due to the torque produced by gravity, an oscillatory motion about the equilibrium is observed.

In order to prove the validity of the linearized model, linear parametric identification techniques were applied to the linearized form of Eq. 4:

$$(I_{xx} + m_{44})\dot{p} = k_p p + \tau_x \quad (6)$$

where the torque τ_x is only due to the effect of pectoral fin lift production, that can be modeled, assuming identical morphology for both pectoral fins, as

$$\tau_x = \frac{1}{2}\rho A C_L d(U_\ell^2 - U_r^2) \quad (7)$$

being ρ the density of the surrounding fluid, A the fin area, C_L the associated lift coefficient and d the distance between

the center of pressure of the fin − where the hydrodynamics forces are supposed to act − and the center of mass of the body − at which rolling moments are calculated −.

For control inputs, we have tested both the amplitude and frequency of fin kinematics. For example, one control variable can be the ratio between the amplitudes of the two pectoral fins, resulting in the following kinematics:

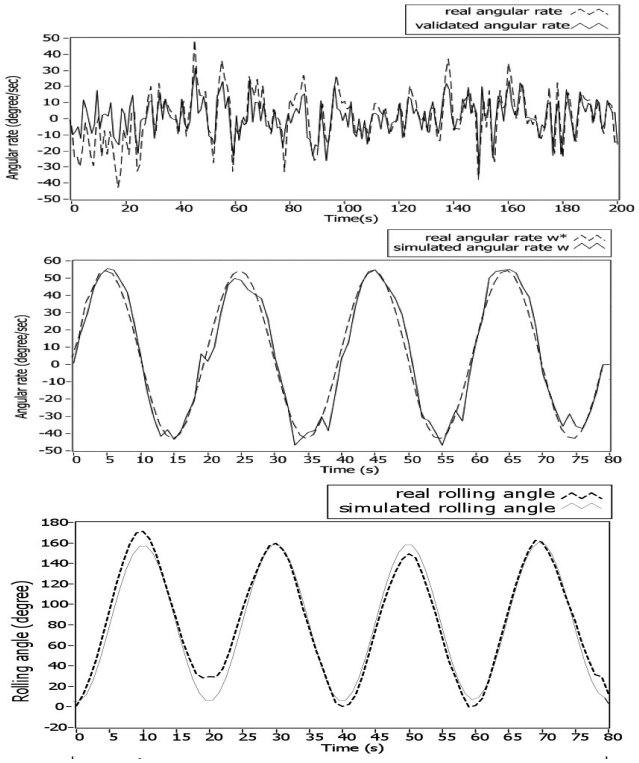

Fig. 3: Model validation through different sets of data. *Top*: angular rate corresponding to a white noise input $u(t) \sim \mathcal{N}(0, 0.3)$. *Center*: angular rate for a sinusoidal input signal at frequency $f = 0.05Hz$. *Bottom*: Rolling angle for the same sinusoidal motion.

$$\begin{cases} \beta_\ell(t) &= \alpha(0.5 + u(t))\sin(\omega t) \\ \beta_r(t) &= \alpha(0.5 - u(t))\sin(\omega t) \end{cases} \qquad u(t) \in [-0.5,\ 0.5] \tag{8}$$

where β_l and β_r are, respectively, the left and right fin angles, and α is the amplitude (here considered to be constant). Thus, by integrating the resulting torque over a finbeat period:

$$\bar{\tau}_x = \frac{1}{2}\rho A C_L d \int_0^T (U_\ell^2 - U_r^2)\, dt = k_f u(t) \tag{9}$$

where k_f is constant. The Laplace transform of the linearized system is then

$$G(s) = \frac{\Phi(s)}{U(s)} = \frac{k_f}{s\left[(I_{xx} + m_{44})s + k_p\right]} \tag{10}$$

By removing the pure integrator, in order to deal with a stable system, the parametric identification based on white noise input ($u(t) \sim \mathcal{N}(0, 0.3)$) shows good agreement between the proposed linear model and the real system, as shown in the validation data in Fig. 3.

In order to control the system on a desired setpoint a PD controller was implemented, assuming that the linear model is a close approximation of the real system. Considering the identified transfer function

$$G(s) = \frac{21.001}{s(s + 1.923)} \tag{11}$$

a PD controller was designed by means of Bode plot method (see Fig. 4), and using a phase margin of $\gamma = 45$ to improve the stability.

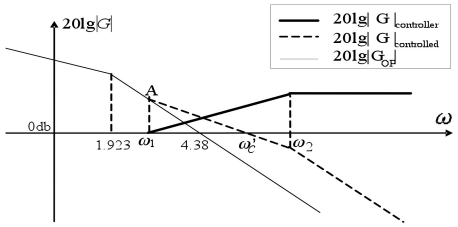

Fig. 4: Bode plot of the controller and the open and closed loop system.

IV. Control Design and Experimental Results

A fish prototype [12], [13], [14], modeled after the boxfish, an *Ostraciiform* coral reef dweller [15], [16], [17], [18], [11], was employed to test the control algorithms. To this end it was equipped with two InvenSense IDG300 dual-axes gyroscopes (with a resolution of 2.44°/s) and an Analog Devices ADXL330 3-axes accelerometer (with a resolution of $6.78\text{m}g$) to provide the sensor feedback (Fig. 5). Control inputs are calculated based on the only attitude estimation from the IMU sensors, and fed back to the PD controller previously designed.

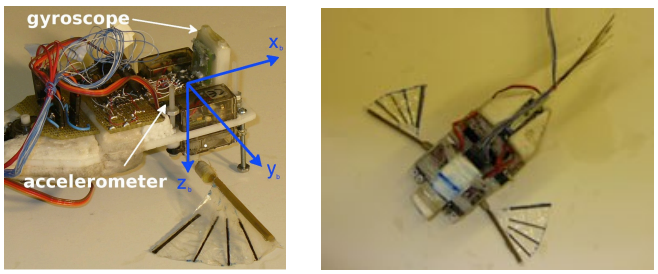

Fig. 5: The fish platform, consisting of electronics, sensors and actuators. The body-fixed coordinate system is also shown.

In the tethered experiments, the model was mounted on a holder and set free to rotate about the roll (x) and yaw (z) axes (see Fig. 6). The holder included two MAE-3 US-Digital angular sensors to measure exact angular displacement. The accelerometers were used to measure the static gravity acceleration, while the gyroscopes provided the angular rate with respect to the three axes in the body reference frame.

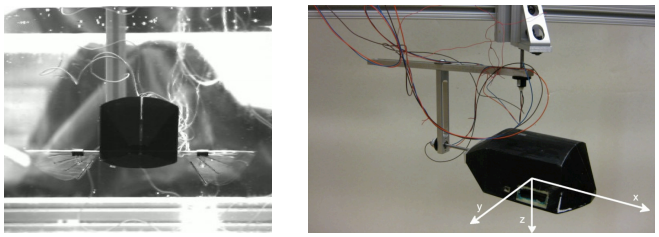

Fig. 6: The boxfish-like hull encasing the model and the 2 DoF holder used in the tethered roll/yaw control experiments.

The results of attitude estimation from the complementary filter [19] are shown in Fig. 7 and the associated sensor readouts are shown in Fig. 8 and 9. The plots show rapid convergence of the estimated angles to the true angles in the first half second of the experiments when the body frame is kept fixed, and then they remain very close to the true angles also during the body motion.

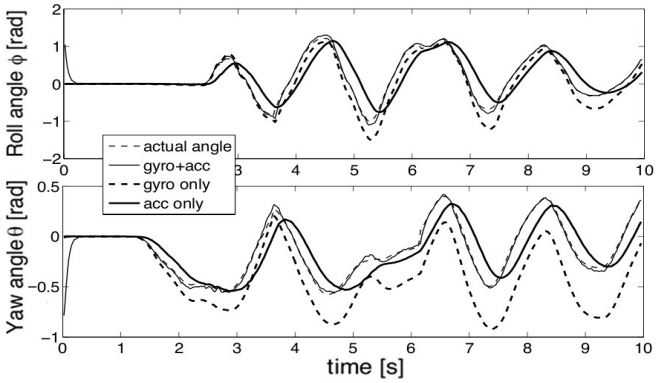

Fig. 7: Comparison between the actual roll angle (*top*) and pitch angle (*bottom*) and three different estimations evaluated using the only accelerometers data, the only gyroscopes data or both.

The effectiveness of sensor fusion is best appreciated by removing either the gyros or the accelerometers from the filter. In the first case, the removal of the gyros results in an evident low pass behavior of the estimated angles which exhibit a time lag as compared to the true angle. Differently, if only gyros are used, the estimated angles have rapid response to body motion, but they incurs in a drift that overtime leads to large offsets as compared to the true angles. The complementary filter, as explained above, fuse the benefits from both sensor modality giving rise to a filter with a very high bandwidth.

Roll control with tethered robot.

Both simulations (Fig. 10) and experimental results (Fig. 11) proved the controller modeled on the linearized system to be effective, even in the presence of external disturbances, such as lateral movements or currents.

The evidence of a precise relation between roll angle and yaw rate was experimentally observed and reported in Fig. 12:

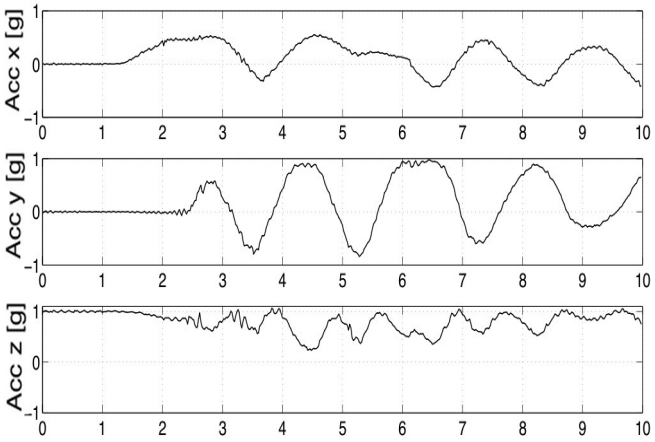

Fig. 8: Accelerometers readouts. Readings are normalized with respect to gravity acceleration g.

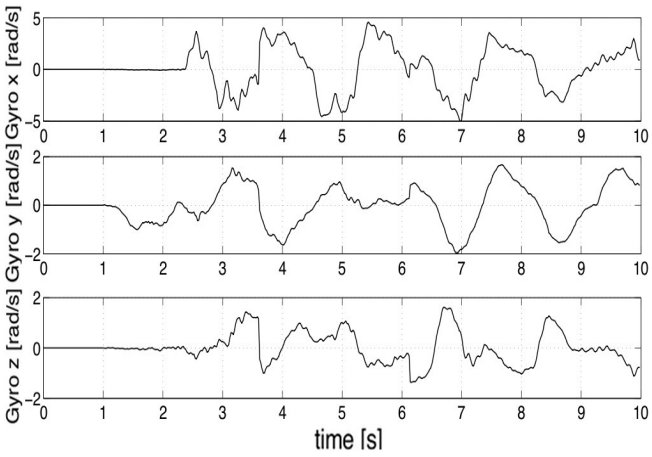

Fig. 9: Gyroscopes readouts.

By controlling the roll angle with pectoral fins it can be noticed that the yaw angle increases linearly, with a constant rate proportional to the relative roll angle.

Assuming that this linear relation holds, it is therefore possible to control the AUV orientation in the yaw plane through its roll angle, as demonstrated by the results shown in Fig. 13. Four different setpoints were chosen as reference for the yaw angle, and the roll control angle was saturated at $\phi_{sat} = \pi/3$, this producing a constant yaw rate before settling to the setpoint.

Banked turn with roll/yaw coupling in free swimming.

The results presented above were limited to one or two degrees of freedom, and consequently their validity needs to be proved in the case of a freely moving[1] AUV as well. Therefore it is important to state whether the proposed pectoral fin control introduces any recoil movement by

[1]The robot was still tethered, since an external power source was required, but the choice of particularly flexible and thin wires allowed an adequate decoupling between the base of the wire and the vehicle, making the disturbance negligible compared to the overall dynamics.

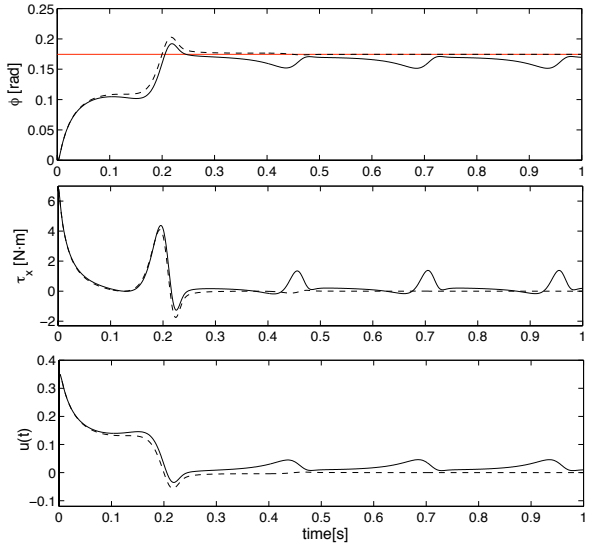

Fig. 10: Simulation results for the roll control of model 5; from *top* to *bottom*: roll angle $\phi(t)$, control torque $\tau_x(t)$ and control input $u(t)$ for the neutrally buoyant case (dashed line) and for the bottom-heavy case (solid line).

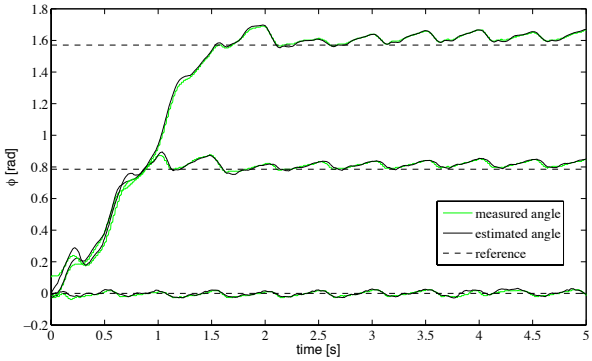

Fig. 11: Data collected during three roll stabilization experiments, respectively at $\phi_{ref} = 0$, $\phi_{ref} = \pi/4$ and $\phi_{ref} = \pi/2$ (*dashed lines*). The estimation (*black lines*) calculated in real time via the sensor fusion algorithm is compared to the actual angle (*green lines*), measured on the holder with MAE-3 angular sensor.

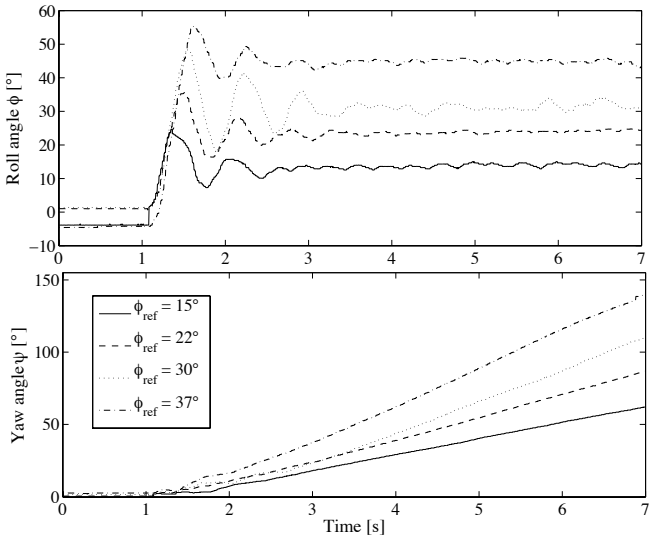

Fig. 12: Roll (*top*) and yaw (*bottom*) angles measured by the respective angular position sensors in four different roll control experiments: the yaw angle varies in a linear fashion, with slope proportional to the relative roll angle.

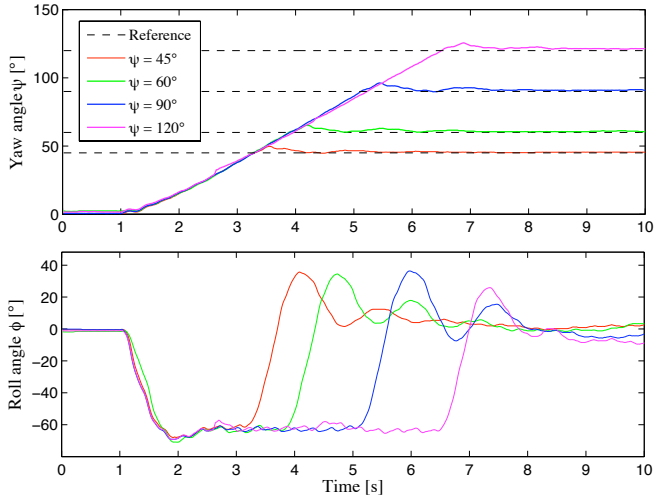

Fig. 13: Yaw (*top*) and roll (*bottom*) angles in 4 tries with different reference angles ψ. The rolling movement is used to control the AUV orientation in the steering plane.

influencing the overall attitude or not. In fact an evident correlation between roll and yaw angles was experimentally observed. This is primarily to be attributed to the lift force generated by pectoral fins when the AUV is tilted in the roll axis and the gravity force does not completely compensate for it. In Fig. 14 the estimated Euler angles of the freely moving AUV during a 20s experiment are shown: the linear controller presented in the previous paragraph was used to track the following roll angle

$$\phi_{ref}(t) = \frac{\pi}{2} \sin 2\pi f t \tag{12}$$

whose frequency f was set to 0.2Hz. The relation between rolling oscillations and yaw orientation suggests the the possibility to control the AUV in the steering plane through the roll angle; this means that the control of a neutrally buoyant AUV in the steering plane would be possible with the only use of pectoral fins. This was demonstrated by a tank experiment (see Fig. 15) in which the robot successfully completed several loops around the tank, with fairly small radius of curvature.

V. Conclusion and Future Work

In this work we presented sensory feedback control results for attitude control in a bio-inspired pectoral fin driven robotic fish. The control algorithm relies on a robust and

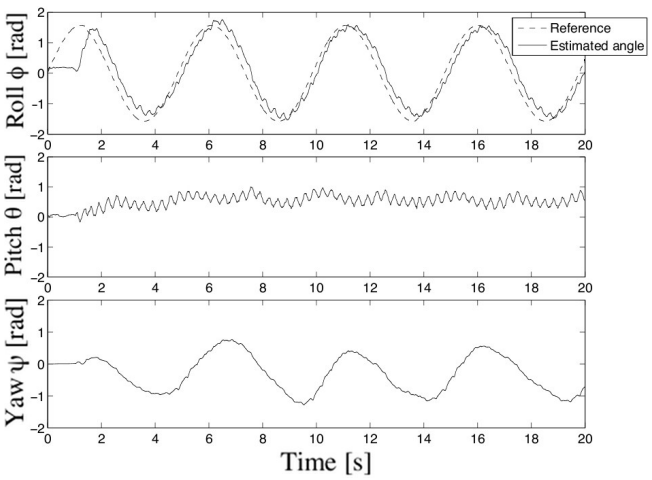

Fig. 14: Euler angles estimated with the sensor fusion algorithm in the 6 dof roll control experiment, with a sinusoidal signal as a reference. Between $t_1 = 0s$ and $t_2 = 1s$ sensors calibration is performed.

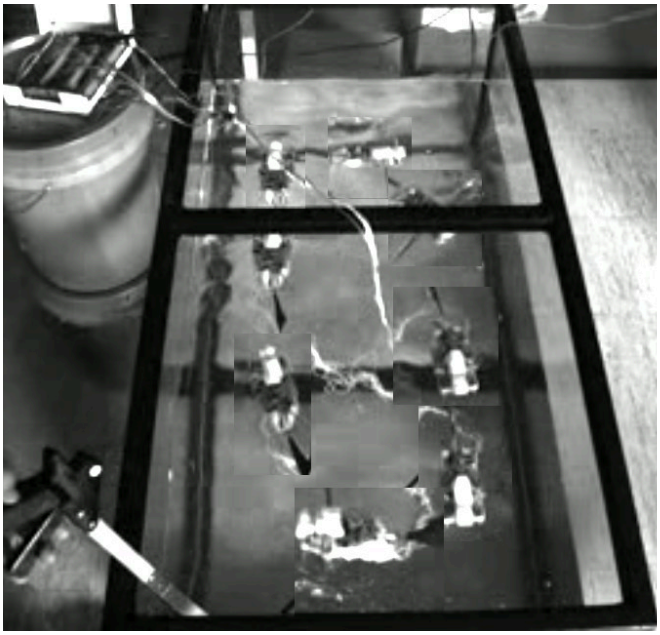

Fig. 15: The model is autonomously swimming along the borders of the tank (frames sampled every 3s), providing both thrust and moments required for turning maneuvers with the only use of the pectoral fins.

computationally efficient sensory feedback, based on a complementary filter fusing data from different Inertial IMU sensors. We presented the effective roll control on tethered and freely swimming robotic fish. While combining roll/yaw coupling, more complicated maneuvers such as a banked turn can be realized on the robot. On-going and future work includes actuating the caudal fin as a propulsion at high speed while as a steering rudder at low speed. The effect of fin-fin interaction and more aggressive maneuvers are under investigation as well.

REFERENCES

[1] M. Dickinson, C. Farley, R. Full, M. Koehl, R. Kram, and S. Lehman, "How animals move: an integrative view," *Science*, vol. 288, no. 5463, pp. 100–106, 2000.

[2] M. Sfakiotakis, D. Lane, and B. Davies, "Review of fish swimming modes for aquatic locomotion," *IEEE Journal of Oceanic Engineering*, vol. 24, no. 2, pp. 237–252, 1999.

[3] G. Lauder and P. Madden, "Learning from fish: kinematics and experimental hydrodynamics for roboticists," *International Journal of Automation and Computing*, vol. 3, no. 4, pp. 325–335, 2006.

[4] J. Tangorra, S. Davidson, I. Hunter, P. Madden, G. V. Lauder, H. Dong, M. Bozkurttas, and R. Mittal, "The development of a biologically inspired propulsor for unmanned underwater vehicles," *IEEE Journal of Oceanic Engineering*, vol. 32, no. 3, pp. 533–550, 2007.

[5] K. Low, S. Prabu, J. Yang, S. Zhang, and Y. Zhang, "Design and initial testing of a single-motor-driven spatial pectoral fin mechanism," *Proceedings of the 2007 IEEE International Conference on Mechatronics and Automation*, pp. 503–508, 2007.

[6] E. Mbemmo, Z. Chen, S. Shatara, and X. Tan, "Modeling of biomimetic robotic fish propelled by a ionic polymer-metal composite actuator," *IEEE International Conference on Robotics and Automation*, 2008.

[7] A. Suleman and C. Crawford, "Design and testing of a biomimetic tuna using shape memory alloy induced propulsion," *Computers and Structures*, vol. 86, pp. 491–499, 2007.

[8] Z. Wang, G. Hang, J. Li, Y. Wang, and K. Xiao, "A micro-robot fish with embedded sma wire actuated flexible biomimetic fin," *Sensors and Actuators*, vol. 144, pp. 354–360, 2008.

[9] A. A. Villanueva, K. B. Joshi, J. B. Blottman, and S. Priya, "A bio-inspired shape memory alloy composite (BISMAC) actuator," *Smart Mater. Struct.*, vol. 19, 2010.

[10] E. Colgate and K. Lynch, "Mechanics and control of swimming: a review," *IEEE Journal of Oceanic Engineering*, vol. 29, no. 3, pp. 660–673, 2004.

[11] J. R. Hove, L. M. O'Brian, M. S. Gordon, P. W. Webb, and D. Weish, "Boxfishes (Teleostei: Ostraciidae) as a model system for fishes swimming with many fins: kinematics," *Journal of Experimantal Biology*, vol. 204, pp. 1459–1471, 2001.

[12] P. Kodati and X. Deng, "Towards the body shape design of a hydrodynamically stable robotic boxfish," in *Proceedings of the 2006 IEEE/RSJ International Conference on Intelligent Robots and Systems*, 2006, pp. 5412–5417.

[13] P. Kodati and X. Deng, "Experimental studies on the hydrodynamics of a robotic ostraciiform tail fin," in *Proceedings of the 2006 IEEE/RSJ International Conference on Intelligent Robots and Systems*, 2006, pp. 5418–5423.

[14] P. Kodati, J. Hinkle, A. Winn, and X. Deng, "Microautonomous robotic ostraciiform (MARCO): hydrodynamics, design and fabrication," *IEEE Transactions on Robotics*, vol. 24, no. 105-117, 2008.

[15] I. K. Bartol, M. S. Gordon, M. Gharib, J. R. Hove, P. Webb, and D. Weish, "Flow patterns around the carapace of rigid-bodied, multi-propulsor boxfishes (Teleostei: Ostraciidae)," *Integrative and Comparative Biology*, vol. 42, pp. 971–980, 2002.

[16] I. K. Bartol, M. Gharib, P. W. Webb, D. Weish, and M. S. Gordon, "Body-induced vortical flows: a common mechanism for self-corrective trimming control in boxfishes," *Journal of Experimantal Biology*, vol. 208, pp. 327–344, 2005.

[17] I. K. Bartol, M. S. Gordon, P. Webb, and M. Gharib, "Evidence of self-correcting spiral flows in swimming boxfishes," *Bioinspiration and Biomimetics*, vol. 3, pp. 1–7, 2008.

[18] M. S. Gordon, J. R. Hove, P. Webb, and D. Weish, "Boxfishes as unusually well-controlled autonomous underwater vehicles," *Phisiological and Biochemical Zoology*, vol. 73, no. 6, pp. 663–671, 2000.

[19] D. Campolo, L. Schenato, L. Pi, X. Deng, and E. Guglielmelli, "Multimodal sensor fusion for attitude estimation of micromechanical flying insects: A geometric approach," in *IEEE/RSJ International Conference on Intelligent Robots and Systems*, 2008, pp. 3859–3864.